# REPORT DOCUMENTATION PAGE

*Form Approved*
*OMB No. 0704-01-0188*



| 1. REPORT DATE *(DD-MM-YYYY)* | 2. REPORT TYPE | 3. DATES COVERED *(From - To)* |
|---|---|---|
| 20 Nov 2006 | REPRINT | |

**4. TITLE AND SUBTITLE**

Gyrotropic guiding-center fluid theory for the turbulent heating of magnetospheric ions in downward Birkeland current regions

**5a. CONTRACT NUMBER**

**5b. GRANT NUMBER**

**5c. PROGRAM ELEMENT NUMBER**
61102F

**6. AUTHORS**

Jasperse, John R., Basu, Bamandas, Lund, Eric J.*, and Bouhram**

**5d. PROJECT NUMBER**
2311

**5e. TASK NUMBER**
SD

**5f. WORK UNIT NUMBER**
A3

**7. PERFORMING ORGANIZATION NAME(S) AND ADDRESS(ES)**

Air Force Research Laboratory /VSBXP
29 Randolph Road
Hanscom AFB, MA 01731-3010

**8. PERFORMING ORGANIZATION REPORT NUMBER**
AFRL-VS-HA-TR-2007-1013

**9. SPONSORING/MONITORING AGENCY NAME(S) AND ADDRESS(ES)**

**10. SPONSOR/MONITOR'S ACRONYM(S)**
AFRL/VSBXP

**11. SPONSOR/MONITOR'S REPORT NUMBER(S)**

**12. DISTRIBUTION/AVAILABILITY STATEMENT**

Approved for Public Release; distribution unlimited.

**13. SUPPLEMENTARY NOTES**

Reprinted from *Physics of Plasmas,* Vol 13, No. 11, 110902 1-13 (2006). © 2006, American Institute of Physics. DOI: 10.1063/1.2264475
* University of New Hampshire, Durham, NH 03824 **CETP-CNRS, 4 Avenue de Neptune, 94107 Saint-Maur Cedex, France

**14. ABSTRACT**

A new fluid theory in the guiding-center and gyrotropic approximation derivable from the ensemble-averaged Vlasov-Maxwell equations. that included the effect of wave-particle interactions for weakly turbulent, weakly inhomogeneous, nonuniformly magnetized plasma was recently given by Jasperse, Basu, Lund, and Bouhram [Phys. Plasmas **13**, 072903 (2006)]. In that theory, the particles are transported in one spatial dimension (the distance $s$ along the magnetic field) but the turbulence is two-dimensional. In this paper, which is intended as a sequel, the above theory is used for quasisteady conditions to find: (1) a new formula for the perpendicular ion-heating rate per unit volume $\dot{W}_{i\perp}(s)$, where $\dot{W}_{i\perp}(s)$ decreases for large s by what we call the "finite ion gyroradius effect"; and (2) a new formula for the perpendicular ion temperature at low altitudes, $T_{i\perp}(s)$. Parametrized calculations for $T_{i\perp}(s)$ are also given.

**15. SUBJECT TERMS**

Birkeland current turbulent heating magnetospheric ions guiding-center
Inhomogeneous, magnetized plasma

| 16. SECURITY CLASSIFICATION OF: a. REPORT | b. ABSTRACT | c. THIS PAGE | 17. LIMITATION OF ABSTRACT | 18. NUMBER OF PAGES | 19a. NAME OF RESPONSIBLE PERSON |
|---|---|---|---|---|---|
| UNCL | UNCL | UNCL | | | Bamandas Basu |
| | | | | | 19B. TELEPHONE NUMBER *(Include area code)* |

**Standard Form 298** (Rev. 8/98)
Prescribed by ANSI Std. Z39.18

PHYSICS OF PLASMAS **13**, 112902 (2006)

# Gyrotropic guiding-center fluid theory for the turbulent heating of magnetospheric ions in downward Birkeland current regions. II

John R. Jasperse and Bamandas Basu
*Air Force Research Laboratory, Space Vehicles Directorate, Hanscom AFB, Massachusetts, 01731*

Eric J. Lund
*Space Science Center, University of New Hampshire, Durham, New Hampshire, 03824*

Mehdi Bouhram
*CETP-CNRS, 4 Avenue de Neptune, 94107 Saint-Maur Cedex, France*

(Received 12 September 2006; accepted 21 September 2006; published online 20 November 2006)

A new fluid theory in the guiding-center and gyrotropic approximation derivable from the ensemble-averaged Vlasov-Maxwell equations that included the effect of wave-particle interactions for weakly turbulent, weakly inhomogeneous, nonuniformly magnetized plasma was recently given by Jasperse, Basu, Lund, and Bouhram [Phys. Plasmas **13**, 072903 (2006)]. In that theory, the particles are transported in one spatial dimension (the distance $s$ along the magnetic field) but the turbulence is two-dimensional. In this paper, which is intended as a sequel, the above theory is used for quasisteady conditions to find: (1) a new formula for the perpendicular ion-heating rate per unit volume $\dot{W}_{i\perp}(s)$, where $\dot{W}_{i\perp}(s)$ decreases for large $s$ by what we call the "finite ion gyroradius effect"; and (2) a new formula for the perpendicular ion temperature at low altitudes, $T_{i\perp}(s)$. Parametrized calculations for $T_{i\perp}(s)$ are also given. © *2006 American Institute of Physics.*
[DOI: 10.1063/1.2364475]

## I. INTRODUCTION

In Ref. 1, hereafter referred to as I, a new fluid theory was presented in the guiding-center and gyrotropic approximation that included the effect of wave-particle interactions for weakly turbulent, weakly inhomogeneous, nonuniformly magnetized plasma. It is the object of the present paper to use the new theory for quasisteady conditions to derive a formula for the perpendicular ion-heating rate per unit volume $\dot{W}_{i\perp}(s)$, and the perpendicular ion-temperature profile at low altitudes $T_{i\perp}(s)$, for a downward Birkeland current region. The present paper is intended as a sequel to I.

The Birkeland currents are a system of upward and downward magnetic field-aligned electrical currents in the auroral zone that flow between the magnetosphere and the ionosphere where particle-number flux, momentum flux, and energy flux are exchanged. For an early study of the statistical properties of the Birkeland currents using TRIAD satellite data (see Ref. 2).

Over the years, much progress has been made in ionospheric plasma physics (see, for example, the recent text by Schunk and Nagy[3] and the references therein). The plasma in most of the Earth's ionosphere is collisional and, as a result, sometimes not too far from equilibrium. By the same token, the use of magnetohydrodynamic (MHD) theory has greatly increased our understanding of solar wind and magnetospheric plasmas, which are essentially collisionless. (See the text by Parker[4] and the references therein for a discussion of the progress that has been made in this area.) However, it is well known that when an **E** field parallel to **B** develops in the Earth's magnetosphere, MHD theory is no longer applicable.[4] Furthermore, magnetospheric plasma is far from equilibrium and is almost always highly turbulent. Since MHD theory cannot be used to treat the field-aligned Birkeland current system, a more general approach is needed.

In I, two traditional approaches to plasma turbulence were briefly discussed. For a review of and references to the theoretical literature in this area, which will not be repeated here (see the Introduction in Ref. 1). There is a vast literature on upward auroral-current regions, which also will not be discussed here (see Ref. 5 for a review of that literature).

The properties of downward auroral-current regions are less explored. They have been observed by the ISIS-2,[6] DE-1,[7] S3-3,[8] FREJA,[9] FAST,[10–13] CLUSTER,[14] and other satellites. From these studies, we see that downward auroral-current regions are often characterized by

(1) diverging electrostatic shocks, downward pointing $E_{\parallel}$;
(2) upflowing low-energy (<few keV) field-aligned electrons;
(3) intense transverse ion heating, energetic ion conics;
(4) small-scale density cavities;
(5) intense extremely low frequency and very low frequency electric-field turbulence and fast bipolar solitary structures;
(6) small fluxes of energetic (>few keV) magnetospheric particles.

Some theoretical work has been carried out using the fluid equations for the current-driven ion-cyclotron instability,[15] particle-in-cell simulations in the electrostatic approximation,[16–20] and velocity-space diffusion models for the problem.[21–24]

In Refs. 21–24, for lack of detailed satellite measurements, it was assumed that magnetospheric ions were heated in downward current sheets by cyclotron resonance with electromagnetic turbulence at the ion cyclotron frequency $\Omega_i$. Now that we have detailed satellite measurements, we are able to determine that, at least for the three cases of FAST satellite data studied in this paper, the turbulence near $\Omega_i$ and its harmonics is electrostatic. Since the parallel wavenumber for electrostatic turbulence is much larger than that for electromagnetic turbulence, an integration over the parallel ion velocity must be performed in order to calculate the turbulent, perpendicular ion-heating rate per unit volume, $\dot{W}_{i\perp}$. This complicates the formula for $\dot{W}_{i\perp}$ (see Sec.VI).

The question arises: Is the one-dimensional fluid theory reviewed in Sec. II of this paper and derived in I applicable to downward Birkeland current regions? The answer is a qualified "yes." This issue is discussed in detail in Sec. III, but it suffices to say here that, as long as we apply the one-dimensional theory to downward current sheets away from the edges of the small-scale, "U-shaped," quasistatic potential structures where the $\mathbf{E}_\perp \times \mathbf{B}$ drift, $u_d$, is small compared to the ion drift along $\mathbf{B}$, $u_i$, the one-dimensional theory applies. Near the quasistatic potential structures, $u_i$ and $u_d$ are comparable, and the one-dimensional theory does not apply. Here, a two-dimensional theory must be used.

As discussed in I, if we could find a renormalized solution of the wave-kinetic and plasma-kinetic equations, the problem would be solved. The renormalized propagator could then be used to find the renormalized distribution functions, dielectric screening function, and the spectral density for the longitudinal electric-field fluctuations for the turbulent plasma. However, the development of a renormalized solution for turbulent, inhomogeneous, nonuniformly magnetized plasma is indeed a formidable problem. The idea that we present in this paper is to bypass this difficult problem by solving the fluid equations, where satellite measurements can be used to specify the turbulent, electric-field fluctuations and where satellite measurements of the low-order velocity moments of the particle distributions can also be used to specify the initial and boundary conditions.

## II. GYROTROPIC GUIDING-CENTER FLUID THEORY FOR THE BIRKELAND CURRENT SYSTEM

In I, we gave a new fluid theory in the guiding-center and gyrotropic approximation derivable from the ensemble-averaged Vlasov-Maxwell equations that included the effect of wave-particle interactions for weakly turbulent, weakly inhomogeneous, nonuniformly magnetized plasma. It was assumed that the turbulence is random and electrostatic, and that the Fokker-Planck operator could be used to calculate the correlation functions that describe the turbulent, wave-particle interactions. At present, the theory has been worked out in one spatial dimension, i.e., the distance $s$ along the geomagnetic field, but the turbulence is two-dimensional since electric-field fluctuations that are both perpendicular and parallel to the geomagnetic field are considered. In this section, we review the theory for the reader's convenience.

From I, the fluid equations in the guiding-center and gyrotropic approximation for continuity, parallel momentum balance, parallel energy balance, and perpendicular energy balance, together with Poisson's equation, are

$$\frac{\partial}{\partial t}n_\alpha + B\frac{\partial}{\partial s}(n_\alpha u_\alpha/B) = 0, \tag{1}$$

$$\frac{\partial}{\partial t}m_\alpha n_\alpha u_\alpha + \frac{\partial}{\partial s}n_\alpha(T_{\alpha\|} + m_\alpha u_\alpha^2) - \frac{1}{B}\frac{dB}{ds}n_\alpha(T_{\alpha\|} + m_\alpha u_\alpha^2 - T_{\alpha\perp}) + q_\alpha n_\alpha \frac{\partial\phi}{\partial s} = \dot{M}_{\alpha\|}, \tag{2}$$

$$\frac{1}{2}\frac{\partial}{\partial t}n_\alpha(T_{\alpha\|} + m_\alpha u_\alpha^2) + \frac{\partial}{\partial s}n_\alpha q_{\alpha\|} - \frac{1}{B}\frac{\partial B}{\partial s}n_\alpha(q_{\alpha\|} - q_{\alpha\perp}) + q_\alpha n_\alpha u_\alpha \frac{\partial\phi}{\partial s} = \dot{W}_{\alpha\|}, \tag{3}$$

$$\frac{\partial}{\partial t}n_\alpha T_{\alpha\perp} + B^2\frac{\partial}{\partial s}(n_\alpha q_{\alpha\perp}/B^2) = \dot{W}_{\alpha\perp}, \tag{4}$$

$$\frac{\partial^2\phi}{\partial s^2} = -4\pi\sum_\beta q_\beta n_\beta, \tag{5}$$

where $s$ is the distance along the geomagnetic field, denoted by $\mathbf{B}$, and $t$ is the time. Gaussian units are used. For particles of type $\alpha$, $n_\alpha$ is the number density, $u_\alpha$ is the parallel drift velocity, $T_{\alpha\|}$ is the parallel temperature, $T_{\alpha\perp}$ is the perpendicular temperature, $q_{\alpha\|}$ is the total parallel energy flux per particle, and $q_{\alpha\perp}$ is the total perpendicular energy flux per particle. By total, we mean the sum of the drift and random parts. We note that $n_\alpha q_{\alpha\|}(n_\alpha q_{\alpha\perp})$ is the total parallel (perpendicular) energy flux for particles of type $\alpha$. The definitions for $q_{\alpha\|}$ and $q_{\alpha\perp}$ *should not be confused with* the heat fluxes per particle, also denoted by $q_\|$ and $q_\perp$ in Braginskii,[25] but defined differently here. The electrostatic potential, denoted by $\phi$, and the low-order velocity moments of the one-particle distribution functions are functions of $s$ and $t$. We have also introduced the quantities $\dot{M}_{\alpha\|}, \dot{W}_{\alpha\|}$ and $\dot{W}_{\alpha\perp}$, where $\dot{M}_{\alpha\|}$ is the rate of transfer of momentum per unit volume for particles of type $\alpha$ due to wave-particle interactions, and $\dot{W}_{\alpha\|}(\dot{W}_{\alpha\perp})$ is the rate of transfer of parallel (perpendicular) energy per unit volume for particles of type $\alpha$ due to wave-particle interactions. The transfer rates are also functions of $s$ and $t$. The $\dot{M}_{\alpha\|}$ are related to the anomalous (turbulent) resistivity for the problem, and $\dot{W}_{\alpha\|}$ and $\dot{W}_{\alpha\perp}$ are the anomalous (turbulent) parallel and perpendicular heating or cooling rates per unit volume for particles of type $\alpha$. The other quantities in (1)–(5) have their usual meaning. The wave-particle transfer rates per unit volume were defined in I as

$$\begin{bmatrix} 0 \\ \dot{M}_{\alpha\parallel} \\ \dot{W}_{\alpha\parallel} \\ \dot{W}_{\alpha\perp} \end{bmatrix} = \int d^3v \begin{bmatrix} 1 \\ m_\alpha v_\parallel \\ m_\alpha v_\parallel^2/2 \\ m_\alpha v_\perp^2/2 \end{bmatrix} \bar{C}_\alpha. \tag{6}$$

Here, $\bar{C}_\alpha$ is the gyrotropic average of $C_\alpha$, which denotes the wave-particle correlation function for particles of type $\alpha$.

In the guiding-center and gyrotropic approximation, we considered a Cartesian velocity-space coordinate system that slowly changes its orientation as $s$ varies along $\mathbf{B}$ so that the $v_z$ axis is always parallel or anti-parallel to $\mathbf{B}$. We then assumed that the fluctuating electric field is random (Markovian), that the length and time scales for the one-particle distribution functions and the two-particle correlation functions separate, and that $\bar{C}_\alpha$ is given by a velocity-space Fokker-Planck operator.[26,27]

$$\bar{C}_\alpha = \frac{1}{2\pi}\int_0^{2\pi} d\varphi \left\{ -\frac{\partial}{\partial \mathbf{v}} \cdot (\mathbf{F}^f_\alpha + \mathbf{F}^p_\alpha)\bar{f}_\alpha + \frac{1}{2}\frac{\partial}{\partial \mathbf{v}}\frac{\partial}{\partial \mathbf{v}} : \mathbf{D}^f_\alpha \bar{f}_\alpha \right\}, \tag{7}$$

where $\varphi$ is the gyrophase angle in the guiding-center coordinate system. Here, $\mathbf{F}^f_\alpha$, $\mathbf{F}^p_\alpha$, and $\mathbf{D}^f_\alpha$ are functionals of $\tilde{\varepsilon}$ and $\langle|\delta\tilde{E}^2|\rangle$, where $\tilde{\varepsilon}$ and $\langle|\delta\tilde{E}^2|\rangle$ are the dielectric screening function and spectral density of the longitudinal electric-field fluctuations for the turbulent plasma, respectively. In (7), $\bar{f}_\alpha$ is the gyrophase average of the one-particle distribution function for particles of type $\alpha$, $\mathbf{F}^f_\alpha$ denotes the friction due to the correlated effect of the electric-field fluctuations on the particle orbit, $\mathbf{F}^p_\alpha$ denotes the friction due to the polarization of the turbulent plasma by a test particle, and $\mathbf{D}^f_\alpha$ denotes the diffusion tensor due to the correlated effect of the electric-field fluctuations on the particle orbit. In I, we also gave explicit expressions for $\dot{M}_{\alpha\parallel}$, $\dot{W}_{\alpha\parallel}$, and $\dot{W}_{\alpha\perp}$ for weak, random, electrostatic turbulence in the guiding-center and gyrotropic approximation. They are:

$$\dot{M}_{\alpha\parallel}(s,t) = \left(\frac{q_\alpha^2\pi}{m_\alpha}\right)\int d^3v \bar{f}_\alpha(s,t,v_\perp,v_\parallel)\int \frac{d^3k}{(2\pi)^3}\sum_{n=-\infty}^{+\infty}\int_{-\infty}^{+\infty} d\omega \left\{ \left(\frac{k_\perp^2}{2k^2}\right)\left(\frac{k_\parallel}{\Omega_\alpha}\right)[J_{n-1}^2(\xi_\alpha) - J_{n+1}^2(\xi_\alpha)]\langle|\delta\tilde{E}^2|(s,t;\mathbf{k},\omega)\rangle \right.$$
$$\left. + \left(\frac{k_\parallel^2}{k^2}\right)k_\parallel J_n^2(\xi_\alpha)\frac{\partial}{\partial\omega}\langle|\delta\tilde{E}^2|(s,t;\mathbf{k},\omega)\rangle + \left(\frac{k_\parallel}{k^2}\right)J_n^2(\xi_\alpha)4m_\alpha \mathrm{Im}[\tilde{\varepsilon}(s,t;\mathbf{k},\omega)^{-1}] \right\}\delta(n\Omega_\alpha + k_\parallel v_\parallel - \omega), \tag{8}$$

$$\dot{W}_{\alpha\parallel}(s,t) = \left(\frac{q_\alpha^2\pi}{m_\alpha}\right)\int d^3v \bar{f}_\alpha(s,t,v_\perp,v_\parallel)\int \frac{d^3k}{(2\pi)^3}\sum_{n=-\infty}^{+\infty}\int_{-\infty}^{+\infty} d\omega \left\{ \left(\frac{k_\perp^2}{2k^2}\right)\left(\frac{k_\parallel v_\parallel}{\Omega_\alpha}\right)[J_{n-1}^2(\xi_\alpha) - J_{n+1}^2(\xi_\alpha)]\langle|\delta\tilde{E}^2|(s,t;\mathbf{k},\omega)\rangle \right.$$
$$\left. + \left(\frac{k_\parallel^2}{k^2}\right)J_n^2(\xi_\alpha)\left[\langle|\delta\tilde{E}^2|(s,t;\mathbf{k},\omega)\rangle + k_\parallel v_\parallel\frac{\partial}{\partial\omega}\langle|\delta\tilde{E}^2|(s,t;\mathbf{k},\omega)\rangle\right] + \left(\frac{k_\parallel v_\parallel}{k^2}\right)J_n^2(\xi_\alpha)4m_\alpha \mathrm{Im}[\tilde{\varepsilon}(s,t;\mathbf{k},\omega)^{-1}] \right\}$$
$$\times \delta(n\Omega_\alpha + k_\parallel v_\parallel - \omega), \tag{9}$$

$$\dot{W}_{\alpha\perp}(s,t) = \left(\frac{q_\alpha^2\pi}{m_\alpha}\right)\int d^3v \bar{f}_\alpha(s,t,v_\perp,v_\parallel)\int \frac{d^3k}{(2\pi)^3}\sum_{n=-\infty}^{+\infty}\int_{-\infty}^{+\infty} d\omega \left\{ \left(\frac{k_\perp^2}{2k^2}\right)n[J_{n-1}^2(\xi_\alpha) - J_{n+1}^2(\xi_\alpha)]\langle|\delta\tilde{E}^2|(s,t;\mathbf{k},\omega)\rangle \right.$$
$$\left. + \left(\frac{k_\parallel^2}{k^2}\right)n\Omega_\alpha J_n^2(\xi_\alpha)\frac{\partial}{\partial\omega}\langle|\delta\tilde{E}^2|(s,t;\mathbf{k},\omega)\rangle + \left(\frac{1}{k^2}\right)n\Omega_\alpha J_n^2(\xi_\alpha)4m_\alpha \mathrm{Im}[\tilde{\varepsilon}(s,t;\mathbf{k},\omega)^{-1}] \right\}\delta(n\Omega_\alpha + k_\parallel v_\parallel - \omega), \tag{10}$$

where $\xi_\alpha = k_\perp v_\perp/\Omega_\alpha$ and $\Omega_\alpha = q_\alpha B/m_\alpha c$ to include the sign of $q_\alpha$. In addition, $J_n(\xi)$ is the usual Bessel function of order $n$, $k_\perp(k_\parallel)$ is the perpendicular (parallel) part of $\mathbf{k}$, and $k^2 = k_\perp^2 + k_\parallel^2$. Here $\mathbf{k}$ is a vector in the guiding-center coordinate system. The other symbols have their usual meaning. We note here that the following symmetries hold: $\langle|\delta\tilde{E}^2|(s,t;\mathbf{k},\omega)\rangle = \langle|\delta\tilde{E}^2|(s,t;-\mathbf{k},-\omega)\rangle$; and $\tilde{\varepsilon}(s,t;\mathbf{k},\omega)^* = \tilde{\varepsilon}(s,t;-\mathbf{k},-\omega)$. We also note that since $\mathbf{B}$ is a function of $s$, so are $\Omega_\alpha$.

Equations (1)–(5) are a set of $4N+1$ equations for the $6N+1$ unknowns: $n_\alpha$, $u_\alpha$, $T_{\alpha\parallel}$, $T_{\alpha\perp}$, $q_{\alpha\parallel}$, $q_{\alpha\perp}$, and $\phi$, where $N$ is the number of plasma constituents. For the set, $2N$ closure conditions are needed. When the model for **B** is given, and when $\bar{f}_\alpha, \langle|\delta\tilde{E}^2|\rangle$ and $\tilde{\varepsilon}$ are specified, then the set of fluid equations, together with (8)–(10) and the closure conditions, may be solved subject to appropriate initial and boundary conditions to give the spatial and temporal evolution of the turbulent plasma. Examples of how this is done for quiescent plasma are given in Secs. VII and VIII of I.

## III. CONDITIONS FOR THE APPLICABILITY OF THE ONE-DIMENSIONAL FLUID THEORY TO THE BIRKELAND CURRENT REGIONS

The question arises: Is the one-dimensional fluid theory reviewed in Sec. II and derived in I applicable to downward Birkeland current regions? The answer is a qualified "yes." From I, we may identify seven conditions that must be satisfied in order to apply the one-dimensional theory to downward current sheets. They are: (1) the length scales for the variation of **B** and **E** must be large; (2) the time scale for the variation of **E** must also be large; (3) the gyrophase average approximation must be valid; (4) the $\mathbf{E}_\perp \times \mathbf{B}$ drifts must be small; (5) the turbulence must be electrostatic; (6) the turbulence must also be weak; and (7) the Fokker-Planck separation of length and time scales must be valid. In this section, we discuss each of these items in consecutive order.

From I, we see that the use of guiding-center coordinates implies the following ordering of length scales:

$$l_{B\|} \gg a_{i\|};\ l_{B\perp} \gg a_{i\perp};\ l_{E\|} \gg a_{i\|};\ l_{E\perp} \gg a_{i\perp}, \tag{11}$$

where the lengths $a_{i\|}$ and $a_{i\perp}$ are defined as $a_{i\|}=|v_{i\|}/\Omega_i|$ and $a_{i\perp}=|v_{i\perp}/\Omega_i|$, and $l$ denotes the length scale for the **B** and **E** variations given in the parallel and perpendicular directions by $l_{Bx}=|(B^{-1}dB/dx)^{-1}|$ and $l_{Ex}=|(E^{-1}dE/dx)^{-1}|$, where $x$ is the distance either parallel or perpendicular to the field. In the three FAST satellite data sets that we have examined in this paper, we found that protons dominate the heavier ion constituents. At FAST altitudes for the three data sets, we find that $u_i \sim 30-70$ km/s, $T_{i\perp} \sim 100-200$ eV, and $B \sim 0.1$ G to give the following average values: $a_{i\|}=40$ m and $a_{i\perp}=1.2\times10^2$ m. In addition, $B(s)\sim B_0(a/s)^3$, $a\sim 6.4\times10^3$ km, $s_2 \sim 10.4\times10^3$ km, where $s_2$ is the satellite altitude, so we estimate that $l_{B\|}/a_{i\|}$ and $l_{B\perp}/a_{i\perp}$ are both $\geq 10^4$. Now consider the **E**-field length scales. In general, there are two cases: the large-scale $\mathbf{E}_\perp$ that leads to convection $\mathbf{E}_\perp \times \mathbf{B}$ drifts as in the Polar Cap and dayside Cusp-Cleft regions, and the small-scale $\mathbf{E}_\perp$ near the edges and sometimes in the middle of the U-shaped, quasistatic potential structures that are known to occur in both upward and downward current sheets.[5,10,28] Consider the small-scale $\mathbf{E}_\perp$. There are two situations: near the shock edges and away from the shock edges. From FAST data for the downward current sheet beginning at UT 1997-01-23/14:37:40 and extending for about 10 s, we find that $E_\perp^{\text{shock}} \leq 0.8$ V/m in $\geq 2.5$ km, so that

$$l_{E\perp}^{\text{shock}}/a_{i\perp} \geq 42. \tag{12}$$

From an examination of the time series of the fluctuating electric field along the satellite track in a downward current sheet for the time period from :07:30 to :07:40 of orbit 1626 shown in Fig. 1 of Ref. 10, we see that for the no-shock region $E_\perp^{\text{noshock}} \leq 11$ mV/m in $\geq 50$ km, so that

$$l_{E\perp}^{\text{noshock}}/a_{i\perp} \geq 8.3\times10^2. \tag{13}$$

Note that the waveform labeled as the dc field in Ref. 10, Fig. 1, is actually sensitive to frequencies up to 1 kHz.[29] Consider $l_{E\|}$. From Ref. 24, Fig. 6 in the auroral zone, $E_\|^{\text{noshock}}$ is $\sim 0.8$ mV/m in $9\times10^2$ km, so

$$l_{E\|}^{\text{noshock}}/a_{i\|} \sim 2.3\times10^4. \tag{14}$$

The conclusion here is that the guiding-center coordinate system may be used even near a small-scale, electrostatic potential structure providing that the length scale for $\mathbf{E}_\perp$ is sufficiently large compared to $a_{i\perp}$.

In the one-dimensional fluid theory given in I, we have assumed that the ensemble-averaged **E** (the background $\mathbf{E}_\perp$ and $\mathbf{E}_\|$) varies on a time scale that is sufficiently large. From I, we see that

$$\tau \gg |2\pi/\Omega_i| \sim 5\times10^{-3}\ \text{s}, \tag{15}$$

where $\tau$ is the time scale for the variation of $\mathbf{E}_\perp$ and $\mathbf{E}_\|$. Thus, the ensemble-averaged **E** field must vary on a time scale that is large compared to $5\times10^{-3}$ s.

In deriving the fluid equations, we have used the gyrophase average of the ion and electron, one-particle distribution functions. In Ref. 23, Fig. 2, a gyrophase-averaged kinetic calculation for the ion conic is compared to the experimental observation in the dayside Cusp-Cleft region near $6\times10^3$ km from the Earth's surface for a downward current sheet. We see that the gyrophase-averaged contours at $10^8$ and $10^7$ s$^3$/km$^6$ are within about 10%–20% of the experimental contours.

In our derivation of the fluid equations in one spatial dimension, we have neglected the $\mathbf{E}_\perp \times \mathbf{B}$ drift compared to the ion drift along **B**. We note here that gradient **B** and curvature **B** drifts are much smaller than $\mathbf{E}_\perp \times \mathbf{B}$ drifts for Birkeland current sheets. First, we consider FAST altitudes. Again, there are two situations: away from a small-scale electrostatic shock and near a small-scale electrostatic shock. From an examination of the time series for the fluctuating electric field along the satellite track beginning at UT 1997-01-23/14:37:40 and extending for about 10 s, we find that $\mathbf{E}_\perp^{\text{noshock}} \leq 11$ mV/m in $\geq 50$ km and $u_i \sim 50$ km/s, so that

$$|u_i/u_d|^{\text{noshock}} \geq 45, \tag{16}$$

where $u_d$ is the $\mathbf{E}_\perp \times \mathbf{B}$ drift velocity. We see that the neglect of $u_d$ is a reasonable approximation for the above data set and the one-dimensional theory applies away from the small-scale, quasistatic potential structure. From Ref. 10, Fig. 2, orbit 1797, we see that $\mathbf{E}_\perp^{\text{shock}} \leq 1$ V/m in $\geq 15$ km, so

$$|u_i/u_d|^{\text{shock}} \sim 1/2. \tag{17}$$

Thus, near a small-scale, quasistatic shock in the long-range potential region of a downward current sheet as shown in Ref. 10, Fig. 2, the neglect of $u_d$ compared to $u_i$ breaks down, and a two-dimensional fluid theory must be used. At CLUSTER altitudes for a downward current sheet, we see from Ref. 14, Fig. 3, that

$$|u_i/u_d|^{\text{noshock}} \geq 150, \tag{18}$$

and that

$$|u_i/u_d|^{\text{shock}} \sim 2.6. \tag{19}$$

The neglect of $u_d$ for a no-shock situation appears valid for altitudes up to $4.3R_E$ (geocentric), but near the shock, the one-dimensional theory still cannot be used at CLUSTER altitudes for downward current sheets.

We have also assumed that the turbulence is electrostatic. In Secs. IV and VI of this paper, we will subtract the Doppler-shifted, quasistatic turbulence from the real, time-dependent turbulence near the proton gyrofrequency and its harmonics and consider the latter signal to be the one that heats the ions by cyclotron resonance. From the wave data for $\delta\mathbf{E}$ and $\delta\mathbf{B}$ near $\Omega_i$, we find that the Poynting flux entering the flux tube at $s_2$ is $\leq 0.01\ \mu\text{W/m}^2$. From the integrated total energy density conservation equation for steady-state conditions given by Eq. (41) of I for electrostatic turbulence, we see that

$$\sum_{e,i} n_\alpha(q_{\alpha\parallel}+q_{\alpha\perp})\Bigg|_{s_1}^{s_2} - \int_{s_1}^{s_2} ds\frac{1}{B}\frac{dB}{ds}\sum_{e,i} n_\alpha(q_{\alpha\parallel}+q_{\alpha\perp}) = \int_{s_1}^{s_2} ds j_\parallel \mathrm{E}_\parallel. \tag{20}$$

On the left-hand side of (20), we can show that $n_e q_{e\parallel}$ dominates the ion total energy flux. Using the satellite particle data at $s_2$ that we will analyze in Secs. IV and VI, and the approximate theory given in Ref. 24 to estimate the second term in (20), we may show that the two terms on the left-hand side of (20) add to give $\sim 14\ \mu\text{W/m}^2$. Since the Poynting flux entering the flux tube at $s_2$ is very small compared to the sum of the two terms on the left-hand side of (20), we conclude that the energy flux to drive the two terms on the left-hand side of (20) is not supplied by the Poynting flux near $\Omega_i$. As a check on this result, we may also use the satellite data for $j_\parallel(s)$ and the approximate theory given in Ref. 24 to estimate $E_\parallel(s)$ on the right-hand side of (20). We obtain, to within experimental error,

$$\int_{s_1}^{s_2} ds\ j_\parallel E_\parallel \cong 14\ \mu\text{W/m}^2. \tag{21}$$

Thus, we conclude that the turbulence at frequencies near $\Omega_i$ and its harmonics is essentially electrostatic, and all of the particle energy flux to within experimental error is supplied by the integral of $j_\parallel E_\parallel$ on the flux tube and not by electromagnetic waves near $\Omega_i$ propagating in from outside the flux tube.

In deriving expressions for the turbulent wave-particle transfer rates in I, we have made the weak turbulence approximation. This implies that the fluctuating quantities are ordered by

$$|\delta f_\alpha/f_\alpha| \sim |\delta n_\alpha/n_\alpha| \sim |q_\alpha\delta\phi/T_\alpha| \sim (2^{1/2}/k\lambda_\text{D}) \times(\delta E^2/8\pi n_\alpha T_\alpha)^{1/2} \ll 1, \tag{22}$$

where $\lambda_\text{D}$ is the Debye length, and $k$ is an average or "characteristic" wavenumber for the turbulence. Using the notation $W=\delta E^2/8\pi nT$, we see that for weak turbulence, $W^{1/2} \ll 1$. For the FAST data set beginning at UT 1997-01-23/14:37:40, we see that $n_i \sim 1-3\ \text{cm}^{-3}$, $T_{i\perp} \sim 100-200$ eV, $\delta E^2 \sim 2.1\times 5.1\times 10^{-5}\text{V}^2/\text{m}^2$. We find that $W\sim 9.9\times 10^{-6}$, and therefore

$$W^{1/2} \sim 3.1\times 10^{-3} \ll 1. \tag{23}$$

In (22), $k\lambda_\text{D}$ is an unknown parameter that depends on the saturated state of the turbulent, inhomogeneous, nonuniformly magnetized plasma. If we accept results from a particle simulation for simplified boundary conditions in a homogeneous medium,[18] we can then estimate that $k\sim k_\perp$ and $k_\perp\lambda_\text{D}\sim 0.1$, so that $2^{1/2}/k\lambda_\text{D}\sim 14$. As long as $2^{1/2}/k\lambda_\text{D}$ is not too much larger than this for realistic conditions on downward current sheets, the above data set satisfies the ordering given by (22).

The use of the Fokker-Planck method to evaluate the interaction between the particles and the turbulence also assumes that the length and time scales between the one-particle distribution functions (and their moments) and the correlation functions for the electric-field fluctuations separate. In Sec. VI of I, we assumed that $l_1 \gg l_2 \sim \lambda_{\text{D}e}$ and $\tau_1 \gg \tau_2 \sim \tau_\text{ac}$. Here, $\tau_\text{ac}$ is the autocorrelation time for the random electric-field fluctuations in the magnetized plasma. At FAST altitudes, $\lambda_{\text{D}e}\sim 20-50$ m and $\tau_\text{ac} \ll 2\pi/\Omega_i \sim 5\times 10^{-3}$ s, so that $l_1 \gg 20-50$ m and $\tau_1 \geq 5\times 10^{-3}$ s. This means that the low-order velocity moments of $\bar{f}_\alpha$ may vary on a time scale on the order of $5\times 10^{-3}$ s or slower. These assumptions imply that if large-amplitude coherent structures (waves or solitons) at frequencies near $\Omega_i$ and its first few harmonics are present and $\tau_2$ becomes large compared to $\tau_\text{ac}$ for the random fluctuations, then the theory given in I may not apply.

We conclude in this section that it is reasonable to apply the one-dimensional fluid theory reviewed in Sec. II, with the qualifications stated above, to turbulent ion heating in the long-range potential region away from the edges of the small-scale, quasistatic potential structures that occur in the downward Birkeland current sheets.

## IV. CHARACTERISTICS OF FAST SATELLITE OBSERVATIONS FOR SOME DOWNWARD CURRENT REGIONS

A number of different plasma and wave processes occur in downward current regions. We have selected three FAST data sets (satellite passes in a downward current region) with similar properties. These properties constitute the assumed physical model which we discuss in this section. For a more general discussion of downward current regions (see Refs. 5 and 10).

For downward Birkeland current regions in the Earth's auroral zone, FAST satellite measurements show that there are often four plasma constituents present. There are large densities of low- to intermediate-energy (<few keV) electrons and ions with a drift velocity up the flux tube. The electrons are field-aligned ($T_{e\parallel} \gg T_{e\perp}$) and thermalized ($u_e < v_{e\parallel}$),[10] and the ions have a "conic" shape in $v_\perp - v_\parallel$ phase space,[12] where $T_{i\perp} > T_{i\parallel}$. There is often a small density of high-energy (5–30 keV) ions moving down the flux tube. Sometimes, there is a small density of high-energy (≥few keV) electrons also moving down the flux tube. Since the densities of the high-energy particles at FAST satellite altitudes are small,[10] and since nearly all the current is carried by the low- to intermediate-energy electrons, we neglect the high-energy particles and consider a two-constituent plasma consisting of the low- to intermediate-energy electrons and ions.

Satellite data, particle simulations, and some analytic results show that there are at least four main altitude regions for downward current sheets: (1) a region below the double layer (DL) region where a downgoing ion beam has been observed;[30] (2) one or more strong laminar double layers each with a width of about $10\lambda_{De}-20\lambda_{De}$ at the bottom of the acceleration region;[13,31] (3) a transition region (TR) just above the DL region with a width of about $100\lambda_{De}-200\lambda_{De}$ where the upgoing electron beam is thermalized;[13,19] and (4) a long-range potential region (LRPR) that extends from the top of the TR to several Earth radii and beyond.[12,14,23,24] Statistically, the bottom of the acceleration region (the DL region) occurs during the winter months from about 1600 to 2500 km.[32] The LRPR extends from the top of the TR to at least $4.3R_E$ (geocentric)[14] and probably beyond. CLUSTER data[14] also show that the downward current sheets remain quasisteady on time scales on the order of a few hundred seconds. At FAST altitudes, observations of the VLF saucers, sometimes a signature of the downward current sheets, indicate that the downward sheets remain quasisteady on time scales greater than several tens of seconds.[10] The turbulence in the TR is often strong;[19] in the LRPR it is often weak.

FAST observations of the fluctuating electric field in the LRPR show that there are at least two kinds of turbulence associated with downward auroral-current regions:[5] broadband extremely low frequency (BBELF)[12] and electron solitary wave (ESW).[11] In this paper, we consider only the former. In a brief examination of FAST data, we found three satellite passes where ion heating by ESW turbulence is negligible, but strong BBELF fluctuations are present. These three cases show a frequency spectrum of electric-field fluctuations in the ELF range in the spacecraft frame of reference. The spectrum consists of two components: a weak, roughly power-law background and broad structured peaks in the spectral density ordered by the proton cyclotron frequency. The peaks are due to temporal fluctuations of the electric field in the ion frame, while the power-law background is due to Doppler-shifted, spatially irregular, electric-field structures that are stationary in the ion frame.[33] Subtracting the two signals, we are left with what we interpret as real, time-dependent turbulence in the ion frame.[34] In Fig. 1, we show FAST satellite data at UT=14:37:45.0274 for the spectral density of the longitudinal electric-field fluctuations for the downward current sheet beginning at UT=1997-01-23/14:37:40 and extending for about 10 s. In panel A, we show the satellite observed spectrum and in panel B, the subtracted spectrum. The vertical dashed lines denote the proton gyrofrequency and its first two harmonics in Hertz. In each of the three data sets that we have studied,

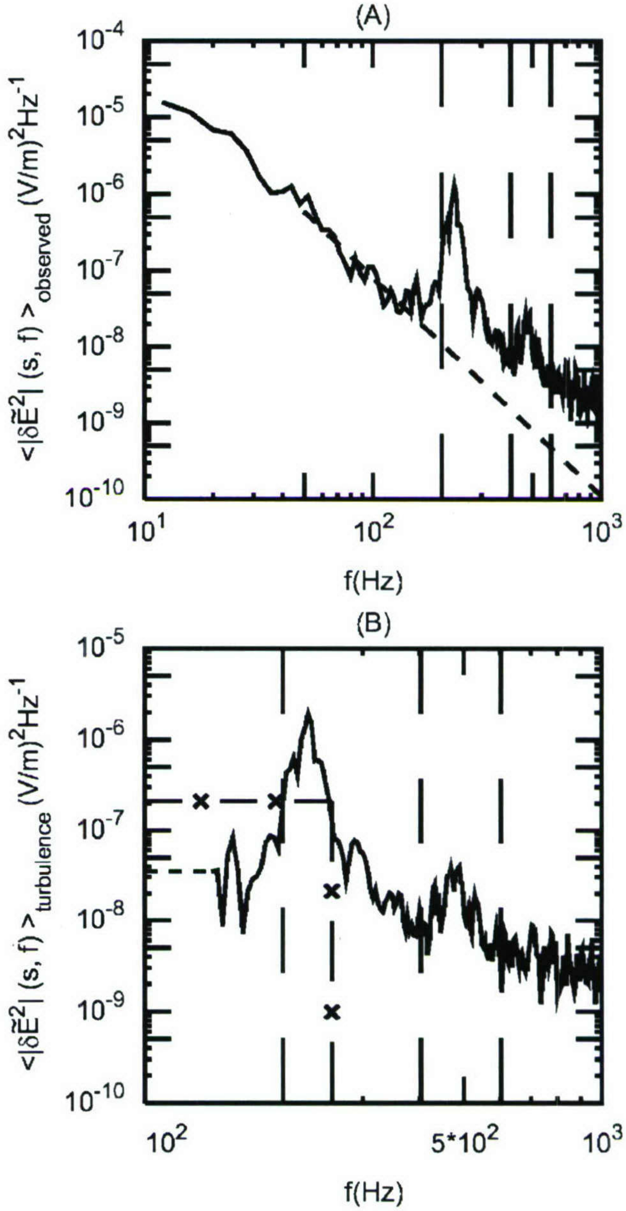


FIG. 1. FAST observations of the spectral density of the longitudinal electric-field fluctuations at UT 1997-01-23/14:37:45.0274: (A) observed spectrum and (B) subtracted spectrum, which is interpreted as time-dependent electrostatic turbulence. Vertical dashed lines denote the proton gyrofrequency and its first two harmonics. The crossed-dashed lines in panel B show the "symmetric window function" approximation discussed in Sec. VI.

we have determined that the turbulence is electrostatic, as discussed in Sec. III.

From Eq. (20) of I,

$$\dot{W}_{e\parallel} + \dot{W}_{e\perp} = -\left\{ \dot{W}_{i\parallel} + \dot{W}_{i\perp} + \frac{\partial}{\partial t}\frac{1}{8\pi}[\langle \delta E_{\perp}^2 \rangle + \langle \delta E_{\parallel}^2 \rangle] \right\}. \tag{24}$$

FAST satellite data in the LRPR show that $\dot{W}_{e\perp} \cong 0$ and that $\dot{W}_{i\perp} > \dot{W}_{i\parallel} \geq 0$. Since we are considering a situation where the ions gain energy from the turbulent wave-ion interaction, and since the turbulence is generated by a plasma instability, then for early times

$$\frac{\partial}{\partial t}\frac{1}{8\pi}[\langle\delta E_{\perp}^{2}\rangle+\langle\delta E_{\parallel}^{2}\rangle]>0. \tag{25}$$

It follows from (24) and (25) that $\dot{W}_{e\parallel}$ is negative. The electrons lose energy as a result of their parallel motion, partly to the heating of the ions and partly to the unstable growing electric-field fluctuations. If a quasisteady solution exists, then the wave term in (24) is zero and $\dot{W}_{e\parallel}\cong-(\dot{W}_{i\perp}+\dot{W}_{i\parallel})$. Since $\dot{W}_{i\perp}+\dot{W}_{i\parallel}$ is positive, then in the quasisteady state, $\dot{W}_{e\parallel}$ is also negative.

Therefore, the physical model that we adopt for the LRPR is that of a magnetic-field-aligned, U-shaped, quasistatic potential structure in which the potential slowly changes as the distance along **B** changes.[5,10,14] We consider a flux tube in the U-shaped region away from any small-scale, electrostatic shocks so that the $\mathbf{E}_{\perp}\times\mathbf{B}$ drift velocity is small compared to the proton drift velocity along **B**, as discussed in Sec. III. For data sets of the above type, we argue that it is the electrostatic turbulence that heats the protons by cyclotron resonance perpendicular to **B** in the LRPR.

In the rest of this paper, we *assume* that a solution of (1)–(5) and (8)–(10) exists that is quasisteady on a time scale of a few hundred seconds.

## V. CLOSURE APPROXIMATION FOR THE PERPENDICULAR ION DYNAMICS

In this section, we discuss the issue of closure. In order to solve for the perpendicular ion-temperature profile $T_{i\perp}(s)$, we must specify a closure condition for the perpendicular ion dynamics. In this paper, we choose the closure $q_{i\perp}(s)\cong u_i(s)T_{i\perp}(s)$ [see (29) below]. In this section, we also discuss Chew, Goldberger, and Low[35] (CGL) closure, where it is assumed that $T_{i\perp}(s)\sim B(s)$, and show that this assumption is not valid when turbulence occurs on downward Birkeland current sheets. For a general discussion of CGL closure (see Ref. 36).

Consider the perpendicular ion dynamics. Equation (4) for the upward drifting ions when there are no fluctuations present is

$$\frac{\partial}{\partial t}n_iT_{i\perp}+B^2\frac{\partial}{\partial s}(n_iq_{i\perp}/B^2)=0. \tag{26}$$

If we choose the closure $q_{i\perp}=u_iT_{i\perp}$, then for low-frequency or for quasisteady phenomena, $\partial T_{i\perp}/\partial t$ is negligible, and we would have

$$\frac{\partial}{\partial s}T_{i\perp}-\frac{1}{B}\frac{dB}{ds}T_{i\perp}=0, \tag{27}$$

where we have used (1). This closure gives the CGL result $(T_{i\perp}\sim B)$ when the fluctuations are negligible. However, when turbulence is present, this closure gives the equation

$$n_iu_i\left(\frac{\partial}{\partial s}T_{i\perp}-\frac{1}{B}\frac{dB}{ds}T_{i\perp}\right)=\dot{W}_{i\perp}. \tag{28}$$

For $u_i>0$ and for $\dot{W}_{i\perp}/n_iu_i>-B^{-1}(dB/ds)T_{i\perp}>0$, the ions will be heated perpendicular to **B** as they move up the **B**-field line. Therefore, we argue that it is reasonable to choose the above closure relation when turbulent ion heating perpendicular to **B** is present. Thus,

$$q_{i\perp}=u_iT_{i\perp}. \tag{29}$$

We consider an electron single-ion plasma with closure given by (29) and approximate (28) by choosing an average value for $u_i$, denoted by $\bar{u}_i$, over the interval $s_1\leq s\leq s_2$:

$$\bar{u}_i\left(\frac{\partial}{\partial s}T_{i\perp}-\frac{1}{B}\frac{dB}{ds}T_{i\perp}\right)=\dot{w}_{i\perp}. \tag{30}$$

Here, $\dot{w}_{i\perp}$ is the perpendicular ion-heating rate per particle denoted by $\dot{w}_{i\perp}=n_i^{-1}\dot{W}_{i\perp}$.

We wish to use the results of Ref. 37 for the ion-temperature relaxation rate to estimate the perpendicular ion-cooling rate for a nonturbulent (collisional) electron-proton plasma with an ion temperature anisotropy $(T_{i\perp}>T_{i\parallel})$ in the limit as $\mathbf{B}\rightarrow 0$. The perpendicular ion-temperature relaxation rate $1/\tau_{i\perp}^{0}$ is defined as

$$dT_{i\perp}/dt=-(T_{i\perp}-T_{i\parallel})/\tau_{i\perp}^{0}. \tag{31}$$

From Ref. 37, we find that at FAST altitudes

$$1/\tau_{i\perp}^{0}\sim 3.1\times 10^{-10}\ \mathrm{s}^{-1}. \tag{32}$$

Since $T_{i\perp}>T_{i\parallel},T_{i\perp}$ is cooled by the thermal fluctuations and the perpendicular ion-cooling rate per particle is approximately

$$\dot{w}_{i\perp(qu)}\sim-3.1\times 10^{-8}\ \mathrm{eV/s}. \tag{33}$$

Using Ref. 37, we have also estimated the electron-ion relaxation rate for quiescent conditions and found it was small compared to $1/\tau_{i\perp}^{0}$, so we neglect it.

We now wish to compare the quiescent cooling rate per particle given by (33) to the adiabatic cooling rate per particle given by the second term on the left-hand side of (30). For FAST satellite altitudes, $B(s)\cong B_0(a/s)^3$, $a\cong 6.4\times 10^3$ km, $s=1.04\times 10^4$ km, $\bar{u}_i\cong 50$ km/s, and $\bar{T}_{i\perp}\cong 150$ eV, so we have

$$\bar{u}_i\frac{1}{B}\frac{dB}{ds}\bar{T}_{i\perp}\cong-2.2\ \mathrm{eV/s}. \tag{34}$$

We conclude that $|\dot{w}_{i\perp(qu)}|$ is indeed very small compared to $|\bar{u}_iB^{-1}(dB/ds)\bar{T}_{i\perp}|$ and that fluctuations at the thermal level play no role in cooling (or heating) the ions in the Earth's magnetosphere. The above argument provides a justification that the CGL closure $T_{\alpha\perp}\sim B$ is valid for quiescent (nonturbulent) magnetospheric plasma in a nonuniform **B** field. However, when there is turbulent ion heating present in the plasma, the CGL closure $T_{i\perp}\sim B$ is not valid.

## VI. ESTIMATE OF THE TURBULENT PERPENDICULAR ION-HEATING RATE

In the last section, we estimated the adiabatic, perpendicular ion-cooling rate per particle for downward current sheets in the LRPR and found that it was about −2.2 eV/s at FAST altitudes. In this section, we will find an approximate formula for the turbulent, perpendicular ion-heating rate per unit volume for quasi-steady conditions using (10). It is given by (49) below and contains what we call the "finite ion gyroradius effect," which acts to reduce the perpendicular ion-heating rate for large values of $s$.

From (10) using symmetry, we see that $\dot{W}_{i\perp}$ is given by a four-dimensional integral and an infinite sum on $n$. If we had satellite data or theoretical formulas for $\langle|\delta\widetilde{E}^2|(s;\mathbf{k},\omega)\rangle$ and $\widetilde{\varepsilon}(s;\mathbf{k},\omega)$ for the turbulent plasma for quasisteady conditions, we could use those expressions together with satellite measurements of $\bar{f}_i(s,v_\perp,v_\parallel)$ to evaluate $\dot{W}_{i\perp}(s)$. However, since such detailed information is lacking, we need to make a number of assumptions and approximations in order to estimate $\dot{W}_{i\perp}(s)$. These assumptions and approximations are discussed in this section.

When an instability is present in the plasma, it is possible for the turbulent fluctuations to grow to be many orders of magnitude larger than those of the thermal fluctuations. Since satellite measurements show electrostatic turbulence in downward current regions, we may infer that one or more instabilities operate on the flux tube and are sustained by maintaining contact with some source of free energy. The expression for $\dot{W}_{i\perp}$ is defined in (6). Using (B24) of I, which relates $\mathbf{F}^f_\alpha$ to $\mathbf{D}^f_\alpha$ by the formula $\mathbf{F}^f_\alpha=(1/2)(\partial/\partial\mathbf{v})\cdot\mathbf{D}^f_\alpha$, we see that the expression for $\dot{W}_{i\perp}$ given by (6), (7), and (10) may be rewritten as

$$\dot{W}_{i\perp}=\int d^3v\frac{1}{2}m_iv_\perp^2\left(\frac{1}{2\pi}\right)\int_0^{2\pi}d\varphi \times\left\{-\frac{\partial}{\partial\mathbf{v}}\cdot\mathbf{F}^p_i\bar{f}_i+\frac{1}{2}\frac{\partial}{\partial\mathbf{v}}\cdot\mathbf{D}^f_i\cdot\frac{\partial}{\partial\mathbf{v}}\bar{f}_i\right\}. \tag{35}$$

Equation (35) has the form of a friction piece given by the first term in the brackets plus a diffusion piece given by the second term. It can be shown that the first term corresponds to the spontaneous emission of plasma waves by the ions and makes a negative contribution to $\dot{W}_{i\perp}$, and the second term corresponds to the stimulated absorption and emission of plasma waves by the ions and makes a positive contribution to $\dot{W}_{i\perp}$. We now introduce the "diffusion approximation for the perpendicular ion dynamics," where we assume that the perpendicular ion energy loss by spontaneous emission is small compared to the perpendicular ion energy gain by stimulated absorption; therefore we neglect the first term in (35) compared to the second. This approximation represents an upper bound on the perpendicular ion-heating rate. Since the ion velocities are small compared to the electron velocities, we argue that this approximation should give a tight upper bound for $\dot{W}_{i\perp}$; i.e., one that is close to the exact value. From (10), we therefore neglect the term proportional to $\mathrm{Im}(1/\widetilde{\varepsilon})$ to obtain for quasisteady conditions

$$\dot{W}_{i\perp}(s)\cong\left(\frac{q_i^2\pi}{m_i}\right)\int d^3v\bar{f}_i(s,v_\perp,v_\parallel)\int\frac{d^3k}{(2\pi)^3}\sum_{n=-\infty}^{n=+\infty}\int_{-\infty}^{+\infty}d\omega\left\{\left(\frac{k_\perp^2}{2k^2}\right)n[J^2_{n-1}(\xi_i)-J^2_{n+1}(\xi_i)]\langle|\delta\widetilde{E}^2|(s;\mathbf{k},\omega)\rangle + \left(\frac{k_\parallel^2}{k^2}\right)n\Omega_iJ_n^2(\xi_i)\frac{\partial}{\partial\omega}\langle|\partial\widetilde{E}^2|(s;\mathbf{k},\omega)\rangle\right\}\delta(n\Omega_i+k_\parallel v_\parallel-\omega). \tag{36}$$

FAST satellite data for the ion-distribution function show that it has a conic shape in $v_\perp - v_\parallel$ space. Therefore, we are led to approximate $\bar{f}_i$ by a "pancake-shaped function"

$$\bar{f}_i(s,v_\perp,v_\parallel)\cong\bar{f}_i\left[s,v_\perp,\frac{(v_\parallel-u_i)^2}{2v_{i\parallel}^2}\right], \tag{37}$$

where $\bar{f}_i$ is a spread-out function of $v_\perp(T_{i\perp}>T_{i\parallel})$ and a peaked function around $v_\parallel=u_i$, where $u_i$ is positive for ions flowing up the flux tube. This is a reasonable approximation for $\bar{f}_i$ at lower altitudes before it becomes folded up by the action of the mirror force term in (2) at higher altitudes. We now integrate (36) on $v_\parallel$ and use integration by parts on $\omega$ in the second term of (36) to obtain

$$\dot{W}_{i\perp}(s)\cong\left(\frac{q_i^2\pi}{m_i}\right)2\pi\int_0^\infty dv_\perp v_\perp\int\frac{d^3k}{(2\pi)^3}\sum_{n=-\infty}^{n=+\infty}\int_{-\infty}^{+\infty}d\omega\frac{1}{|k_\parallel|}\left\{\bar{f}_i\left[s,v_\perp,\frac{(\omega-n\Omega_i-k_\parallel u_i)^2}{2k_\parallel^2v_{i\parallel}^2}\right]\left(\frac{k_\perp^2}{2k^2}\right) \times n[J^2_{n-1}(\xi_i)-J^2_{n+1}(\xi_i)]-\bar{f}_i'\left[s,v_\perp,\frac{(\omega-n\Omega_i-k_\parallel u_i)^2}{2k_\parallel^2v_{i\parallel}^2}\right]\left(\frac{k_\parallel^2}{k^2}\right)\left(\frac{n\Omega_i}{k_\parallel^2v_{i\parallel}^2}\right)(\omega-n\Omega_i-k_\parallel u_i)J_n^2(\xi_i)\right\}\langle|\delta\widetilde{E}^2|(s,\mathbf{k},\omega)\rangle. \tag{38}$$

where $\bar{f}_i'$ is the derivative of $\bar{f}_i$ with respect to its third argument. The following ordering holds for downward currents:

$$0 < u_i < v_{i\parallel} \quad \text{and} \quad 0 < |k_\parallel| < k_\perp, \tag{39}$$

where $k_\parallel$ and $k_\perp$ are average or "characteristic" wavenumbers for the turbulence. Using the approximation that $\bar{f}_i$ is a peaked function of $v_\parallel$ around $u_i$, the ordering in (39), and $k_\perp v_{i\perp}/\Omega_i < 1$, we see that for $T_{i\perp}/T_{i\parallel}$ not too large, the second term in (38) is small compared to the first. Therefore, we may neglect it.

In order to make further progress with the estimation of $\dot{W}_{i\perp}$, we need to make another approximation for the form of $\bar{f}_i$. For our purposes in this section, we may approximate $\bar{f}_i$ in (36) by the product of a Maxwellian in $v_\perp$ times the peaked function of $v_\parallel$:

$$\bar{f}_i(s,v_\perp,v_\parallel) \cong n_i(s)\left(\frac{1}{2\pi v_{i\perp}^2}\right) \times \exp\left(-\frac{v_\perp^2}{2v_{i\perp}^2}\right)\bar{f}_{i\parallel}\left[s,\frac{(v_\parallel - u_i)^2}{2v_{i\parallel}^2}\right], \tag{40}$$

where $v_{i\perp}=v_{i\perp}(s)$, and $\bar{f}_{i\parallel}\{s,(v_\parallel-u_i)^2/2v_{i\parallel}^2\}$ is normalized to 1. As we will see below, the main effect of this approximation is to cut off the $v_\perp$-integration and introduce the function $(2/\beta_i)\Lambda_1(\beta_i)$ into the formula for $\dot{W}_{i\perp}(s)$. Here, $\beta_i=k_\perp^2\rho_i^2=k_\perp^2 v_{i\perp}^2/\Omega_i^2$ and $\Lambda_n(x)=\exp(-x)I_n(x)$, where $I_n(x)$ is the Bessel function of imaginary argument of order $n$. A more accurate treatment of $\bar{f}_i$, for example, a two-dimensional orthonormal expansion in the variables $v_\perp$ and $(v_\parallel-u_i)^2/2v_{i\parallel}^2$, would give a somewhat different cutoff for the $v_\perp$-integration, but should not change the main result in this section. Substituting (40) into (36) and evaluating the $v_\perp$- and $\omega$-integrations, we see that the first term of (36) is

$$\dot{W}_{i\perp}(s) \cong n_i\left(\frac{q_i^2\pi}{m_i}\right)\int_{-\infty}^{+\infty} dv_\parallel \bar{f}_{i\parallel}\left[s,\frac{(v_\parallel-u_i)^2}{2v_{i\parallel}^2}\right]\int\frac{d^3k}{(2\pi)^3}\sum_{n=1}^{\infty}\left(\frac{k_\perp^2}{2k^2}\right)n^2\left(\frac{2}{\beta_i}\right) \times\Lambda_n(\beta_i)\{\langle|\delta\widetilde{E}^2|(s;\mathbf{k},n\Omega_i+k_\parallel v_\parallel)\rangle + \langle|\delta\widetilde{E}^2|(s;\mathbf{k},-n\Omega_i+k_\parallel v_\parallel)\rangle\}. \tag{41}$$

From Sec. II, we see that $\langle|\delta\widetilde{E}^2|(s;-\mathbf{k},-\omega)\rangle = \langle|\delta\widetilde{E}^2|(s;\mathbf{k},\omega)\rangle$. This means that there is as much spectral density at $-\mathbf{k}$ and $-\omega$ as there is at $\mathbf{k}$ and $\omega$. As we mentioned earlier, if we had a satellite measurement of $\langle|\delta\widetilde{E}^2|(s;\mathbf{k},\omega)\rangle$, we could then use it to evaluate the $k$-integration in (41). Since we are, at present, lacking such detailed information about the spectral density, and in order to make further progress with the approximate evaluation of (41), we assume that the $\mathbf{k}$ and $\omega$ variables in the spectral density are approximately separable. In general, we do not expect the spectral density to be exactly separable on $\mathbf{k}$ and $\omega$, even though the plasma may be very turbulent and have no linear dispersion relation. We argue that this approximation should be good enough for the approximate analysis in this section. Therefore, we make the "separation of $\mathbf{k}$ and $\omega$ variables" approximation and write

$$\langle|\delta\widetilde{E}^2|(s;\mathbf{k},\omega)\rangle \cong \langle|\delta\widetilde{E}^2|(s;\mathbf{k})\rangle\langle|\delta\widetilde{E}^2|(s;\omega)\rangle, \tag{42}$$

where $\langle|\delta\widetilde{E}^2|(s;\mathbf{k})\rangle$ is normalized to 1. This approximation means that $\langle|\delta\widetilde{E}^2|(s;-\mathbf{k})\rangle \cong \langle|\delta\widetilde{E}^2|(s;\mathbf{k})\rangle$ and $\langle|\delta\widetilde{E}^2|(s;-\omega)\rangle \cong \langle|\delta\widetilde{E}^2|(s;\omega)\rangle$.

From satellite data for downward currents, we also find that the values of $\langle|\delta\widetilde{E}^2|(s;\omega)\rangle$ as a function of $\omega$ are much smaller near successive values of $\omega=\pm n\Omega_i$, where $n=2,3,\ldots$, than the values of $\langle|\delta\widetilde{E}^2|(s;\omega)\rangle$ near $\omega=\pm\Omega_i$.[34] For example, see Fig. 1. We are led to assume that $\langle|\delta\widetilde{E}^2|(s;\omega)\rangle$ decreases sufficiently fast for large $|\omega|$ so that the low-order, $\omega$-moments of $\langle|\delta\widetilde{E}^2|(s;\omega)\rangle$ exist. As a result, we are also led to make the "symmetric window function" approximation for $\langle|\delta\widetilde{E}^2|(s;\omega)\rangle$, which is defined as

$$\langle|\delta\widetilde{E}^2|(s;\omega)\rangle = \begin{cases} \langle|\delta\widetilde{E}^2|(s)\rangle_{av}, & \text{for } -\omega_0 < \omega < +\omega_0, \\ 0, & \text{otherwise}, \end{cases} \tag{43}$$

where

$$\langle|\delta\widetilde{E}^2|(s)\rangle_{av} = (2\omega_0)^{-1}\int_{-\infty}^{+\infty} d\omega\langle|\delta\widetilde{E}^2|(s;\omega)\rangle. \tag{44}$$

The meaning of this approximation is that the value of $\langle|\delta\widetilde{E}^2|(s;\omega)\rangle$ as a function of $\omega$ is replaced by its average (constant) value for $-\omega_0<\omega<+\omega_0$ and by zero for $|\omega|>\omega_0$, where $\omega_0$ is the half-width of $\langle|\delta\widetilde{E}^2|(s;\omega)\rangle$ in $\omega$ space. The half-width in $\omega$ space is defined as

$$\omega_0 = \int_0^\infty d\omega \omega \langle |\delta\widetilde{E}^2|(s;\omega)\rangle / \int_0^\infty d\omega \langle |\delta\widetilde{E}^2|(s;\omega)\rangle. \tag{45}$$

The symmetric window function as a function of the frequency $f(=\omega/2\pi)$ is shown graphically in Fig. 1 by the crossed-dashed lines in panel B, where $f_0=\omega_0/2\pi=257$ Hz and $\langle|\delta\widetilde{E}^2|\rangle_{av}=2.1\times10^{-7}$ $(\mathrm{V/m})^2\,\mathrm{Hz}^{-1}$ at the satellite altitude. Here, for the three FAST satellite data sets that we have studied, we find that $\omega_0$ is a number that varies from about $1.1\Omega_i$ to $1.4\Omega_i$. From satellite data for the ion velocity moments and from estimates of typical values for $|k_\parallel|$, the following ordering of parameters for downward current regions at FAST altitudes holds: $0<u_i<v_{i\parallel}$ and $|k_\parallel|v_{i\parallel}<\Omega_i\sim\omega_0$. Using this ordering of parameters and the symmetric window function approximation, we see that for the data sets considered, the sum in (41) is dominated by the $n=1$ term and, since $\bar{f}_{i\parallel}\{s,(v_\parallel-u_i)^2/2v_{i\parallel}^2\}$ is normalized to one, the integration on $v_\parallel$ gives

$$\dot{W}_{i\perp}(s)\cong n_i\left(\frac{q_i^2\pi}{m_i}\right)\langle|\delta\widetilde{E}^2|(s)\rangle_{av}\int\frac{d^3k}{(2\pi)^3}\left(\frac{k_\perp^2}{2k^2}\right)\times\left(\frac{2}{\beta_i}\right)\Lambda_1(\beta_i)\langle|\delta\widetilde{E}^2|(s;\mathbf{k})\rangle. \tag{46}$$

We now assume that $\langle|\delta\widetilde{E}^2|(s;\mathbf{k})\rangle$ decreases sufficiently fast for large $k_\perp$ and $|k_\parallel|$, so that its low-order $k_\perp$, and $k_\parallel$ moments exist. Therefore, we are also led to approximate the $k_\perp$- and $k_\parallel$-integrations by making "half-width-in-$k$-space" approximations. This gives

$$\int\frac{d^3k}{(2\pi)^3}\left(\frac{k_\perp^2}{2k^2}\right)\left(\frac{2}{\beta_i}\right)\Lambda_1(\beta_i)\langle|\delta\widetilde{E}^2|(s;\mathbf{k})\rangle\cong\left(\frac{k_{\perp0}^2}{2k_0^2}\right)\times\left(\frac{2}{\beta_{i0}}\right)\Lambda_1(\beta_{i0}), \tag{47}$$

since $\langle|\delta\widetilde{E}^2|(s;\mathbf{k})\rangle$ has been normalized to 1. Here, $\beta_{i0}=k_{\perp0}^2v_{i\perp}^2/\Omega_i^2$ and $k_0^2=k_{\perp0}^2+k_{\parallel0}^2$. The half-widths in $k_\parallel$ and $k_\perp$ space are defined as

$$\begin{bmatrix}k_{\parallel0}\\ k_{\perp0}\end{bmatrix}=(2\pi^2)^{-1}\int_0^\infty dk_\perp k_\perp\int_0^\infty dk_\parallel\begin{bmatrix}k_\parallel\\ k_\perp\end{bmatrix}\langle|\delta\widetilde{E}^2|(s;k_\perp,k_\parallel)\rangle. \tag{48}$$

Using these results, we obtain

$$\dot{W}_{i\perp}(s)\cong n_i\left(\frac{q_i^2\pi}{m_i}\right)\left(\frac{k_{\perp0}^2}{2k_0^2}\right)\left(\frac{2}{\beta_{i0}}\right)\Lambda_1(\beta_{i0})\langle|\delta\widetilde{E}^2|(s)\rangle_{av}. \tag{49}$$

Since $(k_\perp^2/2k^2)(2/\beta_i)\Lambda_1(\beta_i)$ in (46) is a bounded function of $k_\perp$ and $k_\parallel$, and $\langle|\delta\widetilde{E}^2|(s;k_\perp,k_\parallel)\rangle$ is a positive-valued function of $k_\perp$ and $k_\parallel$, this approximation makes sense in light of the first mean value theorem for infinite, one-dimensional integrals (see Ref. 38, Sec. 12), provided that there is no singularity in the iterated $k_\perp$- and $k_\parallel$-integrations. We note that the $k$-integrations in (46)–(48) could contain a logarithmic singularity for large $k$, as was found in the expressions for the relaxation rates for quiescent plasma in Ref. 37. In this case, the integrations were cut off using the "dominant term" approximation of Chandrasekhar.[26] If the low-order $k_\perp$ and $k_\parallel$ moments and the normalization of $\langle|\delta\widetilde{E}^2|(s;\mathbf{k})\rangle$ do not exist, then some other appropriate way of estimating "characteristic" values for $k_\perp$ and $k_\parallel$ needs to be found, so that $k_{\perp0}$ and $k_{\parallel0}$ can be estimated. We also note that in (49), $k_{\perp0}$ and $k_{\parallel0}$ are functions of $s$, and that $v_{i\perp}$ and $\Omega_i$, which appear in $\beta_{i0}$, are also functions of $s$.

In making the above assumptions and approximations, we have reduced the four-dimensional integrations and the infinite sum in (10) to a simple formula. In (49), we see that knowledge of the average spectral density in $\omega$-space, $\langle|\delta\widetilde{E}^2|(s)\rangle_{av}$, the half-width in $\omega$-space, $\omega_0(s)$, the half-widths in $k_\perp$- and $k_\parallel$-space, $k_{\perp0}(s)$, and $k_{\parallel0}(s)$, $\Omega_i(s)$, and $v_{i\perp}(s)$ define $\dot{W}_{i\perp}(s)$. In (49), the function $(2/\beta_{i0})\Lambda_1(\beta_{i0})$ is a monotonically decreasing function of its argument,[38] $\beta_{i0}=k_{\perp0}^2v_{i\perp}^2/\Omega_i^2$. We note that, as the ions are heated perpendicular to $\mathbf{B}$ and move up the flux tube, $v_{i\perp}$ increases from a small value at the bottom of the heating region where $k_{\perp0}v_{i\perp}/\Omega_i<1$, to a larger value at high altitudes where $k_{\perp0}v_{i\perp}/\Omega_i>1$. In this way, the "finite ion gyroradius effect" will act to reduce the perpendicular ion-heating rate for sufficiently large $s$. From FAST satellite data near 4000 km from the Earth's surface, we estimate that $k_{\perp0}^2>k_{\parallel0}^2$ and $\beta_{i0}<1$. In this limit,[38] we find that $(2/\beta_{i0})\Lambda_1(\beta_{i0})\cong1$. Therefore, a rough estimate for (49) at FAST and lower altitudes is

$$\dot{w}_{i\perp av}(s)\cong\left(\frac{q_i^2}{4m_i}\right)\langle|\delta\widetilde{E}^2|(s)\rangle_{av}. \tag{50}$$

Here, the units of $\langle|\delta\widetilde{E}^2|(s)\rangle_{av}$ have been changed from $(\mathrm{V/m})^2$ (angular frequency)$^{-1}$ to $(\mathrm{V/m})^2\,\mathrm{Hz}^{-1}$. We note that (50) is 1/2 the value obtained heuristically[21] from dimensional arguments for the perpendicular ion-heating rate per particle for electromagnetic ion-cyclotron turbulence in downward auroral-current regions. FAST satellite measurements show that for the downward current sheet beginning at UT 1997-01-23/14:37:40 and extending for about 10 s, $\langle|\delta\widetilde{E}^2|\rangle_{av}\sim2.1\times10^{-7}$ $(\mathrm{V/m})^2\,\mathrm{Hz}^{-1}$, so we obtain

$$\dot{w}_{i\perp av}\sim5.0\ \mathrm{eV/s}. \tag{51}$$

We see from (34) that $\dot{w}_{i\perp av}>|\bar{u}_iB^{-1}(dB/ds)\bar{T}_{i\perp}|$ so that $T_{i\perp}(s)$ will increase as the ions move up the flux tube. However, as shown by (49), this increase will not continue indefinitely, and as the ions heat up and $k_{\perp0}v_{i\perp}/\Omega_i\geq1$, $\dot{W}_{i\perp}(s)$ will begin to decrease with increasing $s$ by the finite ion gyroradius effect.

A comparison of (33) for the nonturbulent, very weakly collisional plasma and (51) for turbulent plasma shows that the electric-field fluctuations have grown by about *eight* orders of magnitude due to the presence of one or more instabilities and a source of free energy on the downward, Birkeland current sheet.

## VII. CALCULATION OF THE PERPENDICULAR ION-TEMPERATURE PROFILE AT LOW ALTITUDES

In this section, we solve for the low-altitude, perpendicular ion temperature profile, $T_{i\perp}(s)$ in terms of $\dot{w}_{i\perp av}(s)$ and

$u_i(s)$ for quasisteady conditions. The formula is given by (56) below and parametrized calculations of $T_{i\perp}(s)$ are also given in Fig. 2.

As discussed in Sec. V, the quasisteady equation for $T_{i\perp}(s)$ from (28) is

$$dT_{i\perp}(s)/ds - \{B(s)^{-1}dB(s)/ds\}T_{i\perp}(s) = \dot{w}_{i\perp av}(s)/u_i(s), \tag{52}$$

$$\dot{w}_{i\perp av}(s) = n_i(s)^{-1}\dot{W}_{i\perp av}(s). \tag{53}$$

Equation (52) may be solved by the method of integrating factors. The general solution is

$$\begin{aligned} T_{i\perp}(s) = {} & \exp\left\{-\int ds(-B^{-1}dB/ds)\right\} \\ & \times\int ds\, \dot{w}_{i\perp av}(s)/u_i(s) \\ & \times\exp\left\{+\int ds(-B^{-1}dB/ds)\right\} + C \\ & \times\exp\left\{-\int ds(-B^{-1}dB/ds)\right\}, \end{aligned} \tag{54}$$

where $C$ is a constant that specifies a boundary value for $T_{i\perp}(s)$. We may verify that (54) is a solution of (52) by substitution. From our study in Ref. 23, Fig. 1, we found that $\langle|\delta\tilde{E}^2|(s)\rangle_{av}$ increases with $s$ (as $\Omega_i$ decreases) and is approximately proportional to the increase in $u_i(s)$ with $s$, so that $\dot{w}_{i\perp av}(s)/u_i(s)$ was nearly constant for relatively small distances, $s_2 - s_1 \leq \text{few} \times 10^3$ km. At these altitudes, $k_{\perp 0}v_{i\perp}/\Omega_i < 1$, so that the heating rate was not reduced by the finite ion gyroradius effect. Therefore, we make the approximation

$$\dot{w}_{i\perp av}(s)/u_i(s) \cong [\dot{w}_{i\perp av}(s_1)/u_i(s_1)](s/s_1)^{\gamma}, \tag{55}$$

where $-0.5 \leq \gamma \leq +0.5$. In addition, $-B^{-1}dB/ds \cong 3/s$, so the solution (54) is

$$\begin{aligned} T_{i\perp}(s) = {} & (s_1/s)^3 T_{i\perp}(s_1) + \{\dot{w}_{i\perp av}(s_1)s_1^{-\gamma}/u_i(s_1)(4+\gamma)\} \\ & \times\{s^{1+\gamma} - s_1^{1+\gamma}(s_1/s)^3\}, \end{aligned} \tag{56}$$

where $\dot{w}_{i\perp av}(s_1) \cong (q_i^2/4m_i)\langle|\delta\tilde{E}^2|(s_1)\rangle_{av}$.

In order to show that (56) gives the correct result for $T_{i\perp}(s)$, we would need measurements by two satellites at different altitudes on the same flux tube at the same time. One satellite would give the boundary condition for $T_{i\perp}$ at $s_1$ (the bottom of the LRPR) and values for $\langle|\delta\tilde{E}^2|\rangle_{av}$ and $u_i$, and the other satellite would give the heated values of $T_{i\perp}$ at the satellite altitude $s_2$. Since such coincident measurements are not available, in this section we present parametrized calculations of $T_{i\perp}$ as a function of $\dot{w}_{i\perp av}$ and $u_i$ at $s_2$ and the boundary condition for $T_{i\perp}$ at $s_1$. Satellite data for typical downward current sheets show that the ions are heated from about 20 to 80 eV at the bottom of the LRPR to about 100 to 200 eV at the satellite altitude near 4000 km.[5] Satellite data also show that the bottom of the acceleration region for winter months varies from about 1600 to 2500 km.[32] Therefore,

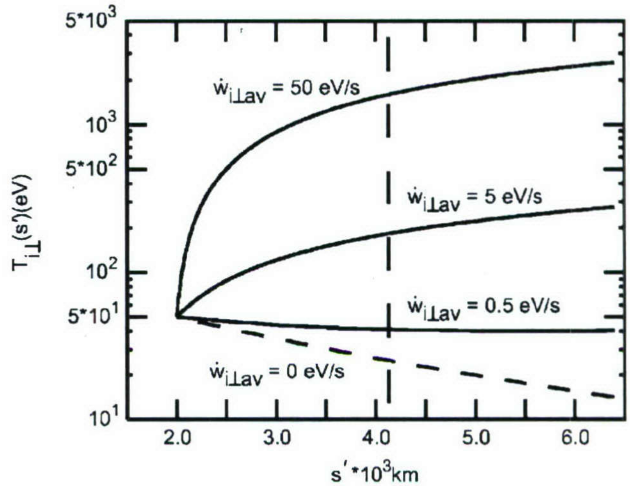


FIG. 2. Solutions of (56) for $T_{i\perp}(s')$ in eV as a function of $s'$ from 2000 to 6400 km for $T_{i\perp}(s_1')=50$ eV, $\gamma=0$, $u_i(s_2')=50$ km/s, for four values of $\dot{w}_{i\perp av}(s_2')$ given by 50, 5.0, 0.5, and 0 in eV/s. The vertical dashed line denotes the satellite altitude at $s_2'=4130$ km.

we choose $s_1=8400$ km ($s_1'=2000$), $T_{i\perp}(s_1')=50$ eV, and $s_2=10\,530$ km ($s_2'=4130$) as the satellite altitude. Here, $s'$ is the distance along **B** from the surface of the Earth, $s'=s-a$, where $a$ is the Earth's radius. From FAST data, we make estimates of $\langle|\delta\tilde{E}^2|\rangle_{av}$ and $u_i$ at the satellite altitude, $s_2'$, and calculate the corresponding value of $\dot{w}_{i\perp av}(s_2')/u_i(s_2')$ using (50). The values of $\dot{w}_{i\perp av}(s_1')/u_i(s_1')$ are inferred from $\dot{w}_{i\perp av}(s_2')/u_i(s_2')$ by using (55) for a choice of the value of $\gamma$. They are then used in (56) to calculate $T_{i\perp}(s')$.

Calculations of $T_{i\perp}(s')$ in eV from $s'=2000$ km to $s'=6400$ km are shown for $T_{i\perp}(s_1')=50$ eV, $u_i(s_2')=50$ km/s, $\gamma=0$, and for four values of $\dot{w}_{i\perp av}(s_2')$ in eV/s, denoted by the dashed and solid curves in Fig. 2. The vertical dashed line shows the satellite altitude at $s_2'=4130$ km. We note that when $\dot{w}_{i\perp av}(s_2')=0$, $T_{i\perp}(s')=T_{i\perp}(s_1')[(s_1'+a)/(s'+a)]^3 \sim B(s')$. This means that when there is no turbulence present, the CGL closure condition, as discussed in Section V, is valid and that $T_{i\perp}$ decreases with $s'$, as shown by the dashed curve in Fig. 2. However, when turbulence is present, Fig. 2 shows that $T_{i\perp}$ increases with $s'$ and the CGL closure condition is no longer valid. Note that the curve for $\dot{w}_{i\perp av}=5$ eV/s produces a $T_{i\perp}$ of 182 eV at the satellite altitude and is typical of the three FAST data sets that we have studied. Note also that if larger heating rates are present, $T_{i\perp}(s_2')$ in the few keV range can occur. Calculations were made for $\gamma=-0.5$ and $\gamma=+0.5$ and the values for $T_{i\perp}(s_2')$ were shifted up and down by about 4% from those given in Fig. 2. Calculations were also made for $T_{i\perp}(s_1')=20$ eV and 80 eV, and for $s_1'=1600$ km and 2500 km, and curves similar to those shown in Fig. 2 were obtained.

The results presented in Fig. 2 can be understood in simple terms. Equation (52) is basically a rate equation for $T_{i\perp}(s')$. Consider the curve in Fig. 2 for $T_{i\perp}(s')$ for $\dot{w}_{i\perp av}(s_2')=5$ eV/s. From (34), we see that the adiabatic cooling rate is about $-2.2$ eV/s and, since the turbulent heating rate is 5 eV/s, the net heating rate is about 2.8 eV/s. From FAST data, the average upward drift of the ions was

50 km/s, so it takes about 43 s for an ion to travel from $s_1'=2000$ km to $s_2'=4130$ km. Thus, the average energy gain for an ion is 43 s$\times$2.8 eV/s=120 eV, and 50 eV+120 eV =170 eV. This compares well with the exact value of 182 eV obtained from (56) for $\gamma=0$.

## VIII. SUMMARY AND DISCUSSION

The main results of this paper are summarized as follows.

(1) In Sec. II, we have reviewed a new fluid theory for the Birkeland current system in the guiding-center and gyrotropic approximation derivable from the ensemble-averaged Vlasov-Maxwell equations that includes the effect of wave-particle interactions in which the particles are transported in one spatial dimension (the distance $s$ along **B**), but the turbulence is two-dimensional since electric-field fluctuations that are both perpendicular and parallel to **B** are considered.

(2) When the turbulence is random and electrostatic, we argue that the one-dimensional fluid theory may be applied in the long-range potential region (LRPR) of a downward Birkeland current sheet on flux tubes away from the edges of any small-scale, U-shaped, quasistatic potential structures, so that the $\mathbf{E}_\perp\times\mathbf{B}$ drift remains small compared to the ion drift along **B** (see Sec. III).

(3) In Sec. V, we use $q_{i\perp}=u_iT_{i\perp}$ to close the perpendicular ion dynamics and present an argument as to why this is a reasonable assumption.

(4) For quasisteady conditions, we have reduced the expression for $\dot{W}_{i\perp}$ from a four-dimensional integral and an infinite sum on $n$, given by (10), to a simple formula, given by (49), by making a number of assumptions and approximations. They are: (a) the "diffusion assumption for the perpendicular ion dynamics"; (b) the approximation of the ion conic in $v_\perp-v_\parallel$ space by a "pancake-shaped function" with the $v_\perp$-dependence given by a Maxwellian; (c) the assumption that $\langle|\delta\tilde{E}^2|(s;\mathbf{k},\omega)\rangle$ is "separable in its **k** and $\omega$ variables"; and (d) the idea that $\langle|\delta\tilde{E}^2|(s;\omega)\rangle$ can be approximated by a "symmetric window function" and that average or "characteristic" values for $k_\perp$ and $k_\parallel$ can be found from $\langle|\delta\tilde{E}^2|(s,\mathbf{k})\rangle$. We argue that (49) gives a reasonable upper bound for $\dot{W}_{i\perp}$. Our analysis leads to the idea that the turbulent, perpendicular ion-heating rate does not increase indefinitely with increasing $s$, but is reduced for large $s$ by the "finite ion gyroradius effect" (see Sec. VI).

(5) In Sec. VII, we gave a new formula for the low-altitude, perpendicular ion-temperature profile, $T_{i\perp}(s')$, and also gave parametrized calculations of $T_{i\perp}(s')$ as a function of $\dot{w}_{i\perp av}(s_2')$ and $u_i(s_2')$ in Fig. 2.

There are other mechanisms by which magnetospheric ions can be heated perpendicular to **B** on auroral field lines beside the one presented in this paper. For a discussion of these processes (see Ref. 5). When ESW turbulence is present in the LRPR of downward current sheets, it is well known that intense ion heating perpendicular to **B** occurs.[11] If ion heating by ESW turbulence is a random process and if a theory for the spectral density of the longitudinal electric-field fluctuations could be developed, then the spectral density could be used to find $\dot{w}_{i\perp}$ for ESW turbulence, and calculations of $T_{i\perp}$ as a function of $s'$ could also be made.

The following picture for the downward Birkeland current region is suggested by satellite observations,[5–14] particle simulations,[16–20] and the analysis in this paper and in Refs. 1 and 21–24. As the current density increases with decreasing altitude, one or more strong double layers[13,16–20,31] develop at an altitude that ranges during winter months from about 1600 to 2500 km from the Earth's surface.[32] The electrons are accelerated upward by the downward pointing, self-consistent $\mathbf{E}_\parallel$ field and some of the ions are dragged upward against the downward pointing $\mathbf{E}_\parallel$ field in order to maintain quasineutrality.[8,16–20,23,24] In the LRPR when ESW turbulence is absent, the ions are heated perpendicular to **B** by cyclotron resonance with electrostatic turbulence near $\Omega_i$ and its harmonics.[1] The ions are gaining perpendicular and parallel energy from the turbulence and the electrons are losing parallel energy to the turbulence, as indicated by (24) and (25) of Sec. IV. In a quasisteady state, the amount of parallel energy lost by the electrons is equal to the amount of perpendicular and parallel energy gained by the ions.[1] In the LRPR, some of the electrons that are accelerated upward by $\mathbf{E}_\parallel$ are driven into the downward direction by the magnetized, turbulent, electron-wave interactions.[1] Since $\dot{W}_{e\perp}\cong 0$, the electrons are actually cooled adiabatically in the perpendicular direction[9,10] as indicated by the perpendicular energy balance equation for the electrons.[1,23,24] Since $\dot{W}_{e\perp}\cong 0$, these equations for the electrons are similar to (26), (27), and (29) of this paper. In the LRPR, this leads to a field-aligned $(T_{e\parallel}\gg T_{e\perp})$ and thermalized $(u_e<v_{e\parallel})$ electron distribution function parallel to **B**,[1,10,23,24] and a heated ion-distribution function $(T_{i\perp}>T_{i\parallel})$ in the directions perpendicular and parallel to **B**.[1,10,12,23,24] In the LRPR, the mirror force acts on the ions [see the third term on the left-hand side of (2)], so as to fold up the ion-distribution function into a conic-shaped distribution in $v_\perp-v_\parallel$ phase space, as the ions move up the flux tube.[12,23,24] In the LRPR for quasisteady conditions, preliminary calculations using (1)–(5) and (8)–(10) show that the self-consistent $\mathbf{E}_\parallel$ is sustained primarily by the mirror force (Alfven-Falthammar) and parallel energy divergence terms in the momentum balance equation given by (2),[1,12,23,24] and that the anomalous resistivity, which is proportional to $\dot{M}_{e\parallel}$, plays a minor role. The above scenario is consistent with FAST and other satellite observations for downward Birkeland current sheets.[6–14,31,32]

We recognize that a two-dimensional fluid theory in the guiding-center coordinate system needs to be developed so that $\mathbf{E}_\perp\times\mathbf{B}$ drifts near the edges of the small scale U-shaped, quasistatic potential structures may be taken into account. An analysis along these lines is currently in progress where we assume that the geomagnetic field is that of a dipole and use dipolar coordinates to express the guiding-center kinetic equations, Poisson's equation, the moment equations, and the wave-particle transfer rates for the turbulent plasma. We also recognize the need to include the effect of electromagnetic turbulence.

It is the main conclusion of this paper that, in the absence of ESW turbulence when structured electrostatic turbulence near $\Omega_i$ and its harmonics is present on downward Birkeland current sheets in the long-range potential region, the ions are heated perpendicular to **B** by cyclotron resonance, and the gyrotropic guiding-center fluid theory presented in this paper gives the perpendicular ion temperature profile at low altitudes for quasisteady conditions.

## ACKNOWLEDGMENTS

We wish to acknowledge important conversations with the following people: J. W. Bonnell, W. J. Burke, C. W. Carlson, T. S. Chang, D. L. Cooke, N. J. Grossbard, K. A. Lynch, D. C. Montgomery, and R. Pottelette.

This work was supported by the Air Force Office of Scientific Research. E. J. L. was partially supported by NASA Grant No. NNG04GP84G.

[1] J. R. Jasperse, B. Basu, E. J. Lund, and M. Bouhram, Phys. Plasmas **13**, 072903 (2006).
[2] T. Ijima and T. A. Potemra, J. Geophys. Res. **83**, 599 (1978).
[3] R. W. Schunk and A. F. Nagy, *Ionospheres: Physics, Plasma Physics, and Chemistry* (Cambridge University Press, Cambridge, UK, 2000).
[4] E. N. Parker, *Spontaneous Current Sheets in Magnetic Fields* (Oxford University Press, New York, 1994).
[5] G. Paschmann, S. Haaland, and R. Treumann, Space Sci. Rev. **103**, 1 (2002).
[6] D. M. Klumpar and W. J. Heikkila, Geophys. Res. Lett. **9**, 873 (1982).
[7] J. L. Burch, P. H. Reiff, and M. Sugiura, Geophys. Res. Lett. **10**, 753 (1983).
[8] D. J. Gorney, Y. T. Chiu, and D. R. Croley, J. Geophys. Res. **90**, 4205 (1985).
[9] M. H. Boehm, J. Clemmons, J. E. Wahlund *et al.*, Geophys. Res. Lett. **22**, 2103 (1995).
[10] C. W. Carlson, J. P. McFadden, R. E. Ergun *et al.*, Geophys. Res. Lett. **25**, 2017 (1998).
[11] R. E. Ergun, C. W. Carlson, J. P. McFadden *et al.*, Geophys. Res. Lett. **25**, 2041 (1998).
[12] K. A. Lynch, J. W. Bonnell, C. W. Carlson, and W. J. Peria, J. Geophys. Res. **107**, 16-1 (2002).
[13] L. Andersson, R. E. Ergun, D. L. Newman *et al.*, Phys. Plasmas **9**, 3600 (2002).
[14] G. T. Marklund, N. Ivchenko, T. Karlsson *et al.*, Nature (London) **414**, 724 (2001).
[15] S. B. Ganguli and P. J. Palmadesso, J. Geophys. Res. **92**, 8673 (1987).
[16] N. Singh, H. Thiemann, and R. W. Schunk, Planet. Space Sci. **35**, 353 (1987).
[17] R. M. Winglee, P. L. Pritchett, P. B. Dusenbery *et al.*, J. Geophys. Res. **93**, 14567 (1988).
[18] F. J. Crary, M. V. Goldman, R. E. Ergun, and D. L. Newman, Geophys. Res. Lett. **28**, 3059 (2001).
[19] M. V. Goldman, F. J. Crary, D. L. Newman, and M. Oppenheim, Phys. Plasmas **7**, 1732 (2002).
[20] N. Singh and I. Khazanov, Geophys. Res. Lett. **30**, 2262 (2003).
[21] T. S. Chang, G. B. Crew, N. Hershkowitz *et al.*, Geophys. Res. Lett. **13**, 636 (1986).
[22] G. B. Crew, T. S. Chang, J. M. Retterer *et al.*, J. Geophys. Res. **95**, 3959 (1990).
[23] J. R. Jasperse, Geophys. Res. Lett. **25**, 3484 (1998).
[24] J. R. Jasperse and N. J. Grossbard, IEEE Trans. Plasma Sci. **28**, 1874 (2000).
[25] S. I. Braginskii, in *Reviews of Plasma Physics*, edited by M. A. Leontovich (Consultants Bureau, New York, 1965), Vol. 1, p. 205.
[26] S. Chandrasekhar, Rev. Mod. Phys. **15**, 1 (1943).
[27] S. Ichimaru, *Statistical Plasma Physics* (Addison-Wesley, Redwood City, 1992).
[28] C. W. Carlson, R. F. Pfaff, and J. G. Watson, Geophys. Res. Lett. **25**, 2013 (1998).
[29] R. E. Ergun, C. W. Carlson, F. S. Mozer *et al.*, in *The Fast Mission*, edited by R. F. Pfaff (Kluwer Academic, Dordrecht, 2001), Vol. 98, p. 67.
[30] C. Cattell, L. Johnson, R. Bergmann *et al.*, J. Geophys. Res. **107**, 1238 (2002).
[31] R. E. Ergun, Y. J. Su, L. Andersson *et al.*, Phys. Rev. Lett. **87**, 045003 (2001).
[32] R. C. Elphic, J. Bonnell, R. J. Strangeway *et al.*, in *Magnetospheric Current Systems*, edited by S. I. Othani *et al.* (AGU, Washington, DC, 2000), Vol. 118, p. 173.
[33] M. Temerin, J. Geophys. Res. **83**, 2609 (1978).
[34] E. J. Lund, J. R. Jasperse, K. A. Lynch, *et al.*, American Geophysical Union Fall Meeting 2005, Abstract # SM41C-1195 [EOS Trans. Am. Geophys. Union **86**, 52 (2005)].
[35] G. F. Chew, M. L. Goldberger, and F. E. Low, Proc. R. Soc. London, Ser. A **236**, 112 (1956).
[36] N. A. Krall and A. W. Trivelpiece, *Principles of Plasma Physics* (San Francisco Press, San Francisco, 1986), pp. 118–122.
[37] S. Ichimaru and M. N. Rosenbluth, Phys. Fluids **13**, 2778 (1970).
[38] S. Gradshteyn and I. M. Ryzhik, *Table of Integrals, Series, and Products* (Academic, New York, 1980).